Journal of The Electrochemical Society

Limitations of Polyacrylic Acid Binders When Employed in Thick LNMO Li-ion Battery Electrodes

To cite this article: Alma Mathew *et al* 2024 *J. Electrochem. Soc.* **171** 020531

Journal of The Electrochemical Society, 2024 **171** 020531

Limitations of Polyacrylic Acid Binders When Employed in Thick LNMO Li-ion Battery Electrodes

Alma Mathew,[1] Wessel van Ekeren,[1] Rassmus Andersson,[1] Matthew J. Lacey,[2] Satu Kristiina Heiskanen,[3] Reza Younesi,[1] and Daniel Brandell[1,z]

[1]*Department of Chemistry-Ångström Laboratory, Uppsala University, 75121 Uppsala, Sweden*
[2]*Scania CV AB, 15187 Södertälje, Sweden*
[3]*Volkswagen AG, 38436 Wolfsburg, Germany*

Polyacrylic acid (PAA) is here studied as a binder material for $LiNi_{0.5}Mn_{1.5}O_4$ (LNMO) cathodes for lithium-ion batteries. When the LNMO electrodes are fabricated with an active mass loading of ~10 mg cm^{-2} (~1.5 mA h cm^{-2}), poor discharge capacity and short cycle life is obtained in full-cells with graphite electrodes. The electrochemical results with PAA are compared with a commonly used water-based binder, sodium carboxymethyl cellulose (CMC), which shows better electrochemical performance. The main cause for these problems in PAA based cells is identified to be the high internal resistance in the initial cycles, caused by factors such as contact resistance, inhomogeneous binder distribution and poor electrolyte wetting of the active material.
 [DOI: 10.1149/1945-7111/ad242b]

Manuscript submitted November 10, 2023; revised manuscript received January 7, 2024. Published February 16, 2024.

Supplementary material for this article is available online

The growing popularity of electric vehicles has led to an increased demand for lithium-ion batteries (LIBs), which are seen as a crucial technology for combating climate change and reducing greenhouse gas emissions. When evaluating the performance of batteries in electric vehicles and other applications, both energy density and power density are important factors to consider. The LIB cathode material $LiNi_{0.5}Mn_{1.5}O_4$ (LNMO) operates at 4.7 V (vs Li/Li$^+$) and has a specific capacity of 147 mAh g^{-1}, which means this material offers an energy density comparable to $Li(Ni_xMn_yCo_z)O_2$ (NMC) cathodes.[1,2] LNMO cathodes also have 3D-ion diffusion channels inherent in the spinel structure, which helps to increase the power density of this material by allowing faster movement of ions within the structure.[3] Moreover, LNMO cathodes are made using raw materials that are more abundant than cathodes that contain cobalt, which makes them more cost-effective and sustainable. Cobalt is also a metal associated with environmental and human rights concerns.[4]

Despite these advantages, batteries with LNMO positive electrodes are prone to comparatively rapid capacity decay, especially in full-cells and at elevated temperatures. This is partly due to the high voltage of operation of LNMO, i.e., ~4.7 V (vs Li/Li$^+$), at which the conventional electrolytes are thermodynamically unstable and can cause harmful side-reactions.[5,6] Transition metal dissolution from the active material in an LNMO cathode can lead to chemical decomposition of electrolyte and/or deposition on the anode, leading to additional side-reactions which can negatively impact the performance of the battery.[7] One strategy to address these issues is to create a stable interphase layer between the LNMO electrode and the electrolyte. This can, for example, be accomplished by using suitable binders in the battery electrodes, which not only hold the active particles together to maintain electrical conductivity and mechanical stability of the electrode, but also affect the surface chemistry of the electrode. Thereby, they act to some degree as an "artificial" interphase layer, as previously demonstrated for both positive and negative electrodes.[8–14]

The overall performance of a battery can be significantly impacted by the performance of the binder, even though it is only present in small amounts. Firstly, the binder needs to strongly adhere to both the active material and the current collector to create a uniform and stable layer that can withstand any mechanical pressure during battery operation. Secondly, the binder should possess chemical and electrochemical stability, or the ability to form a stable passivation layer during the operation of the battery. The binder in an electrode can also have a significant impact on crucial factors for the performance of the electrode, such as an electrode porosity that generates efficient ion and electrolyte transport to the active material, reducing swelling, and good electrolyte wetting.[14–17]

Polyvinylidene difluoride (PVDF) has for a long time been the most common battery electrode binder material due to its good mechanical, electrochemical and chemical properties.[18] However, electrodes processed with PVDF binder use N-Methyl-2-pyrrolidone (NMP), which is a toxic solvent, posing risk to human health and the environment.[19] Moreover, due to its non-polar structure, PVDF forms weak intermolecular interactions with both the active material and the current collector, which can result in mechanical failure and a decline in capacity during long-term cycling.[19] Therefore, water-based binders have emerged in recent years as more sustainable and high-performing alternatives. For example, sodium carboxymethyl cellulose (CMC) is nowadays a common binder primarily explored due to its homogeneous distribution in both positive and negative electrodes.[20,21] In addition, the presence of a carboxymethyl functional group in CMC leads to strong interaction with the active materials through hydrogen bonding, resulting in improved adhesion of the active materials. Other water-based binders under exploration includes but is not limited to polyacrylic acid (PAA), carboxymethyl chitosan, sodium alginate, and polyvinyl acetate.[10,21] The Lewis structures of CMC and PAA, the binders explored in this study, are shown in Fig. 1.

Developing electrodes with high mass-loading and good performance for commercial batteries is a major challenge in the field of LIB electrode development. One of the key difficulties is finding the right combination of binder material and electrode fabrication methods, such as mixing and drying conditions, without compromising the resulting capacity and rate performance. In this study, the focus is on PAA because of its hypothesized capability to create strong hydrogen bonds with the surface of the active component, LNMO, thus providing a strategy for avoiding the detrimental direct contacts between the active material and the electrolyte. Polyacrylates also contain a higher number of carboxyl groups than CMC, which should allow them to more strongly attach to the surface of LNMO particles.[10] Previous studies have investigated the use of PAA and its derivatives in various battery chemistries, often indicating an enhancement in their electrochemical performance as compared to alternatives.[22–27] However, these studies have generally

[z]E-mail: daniel.brandell@kemi.uu.se

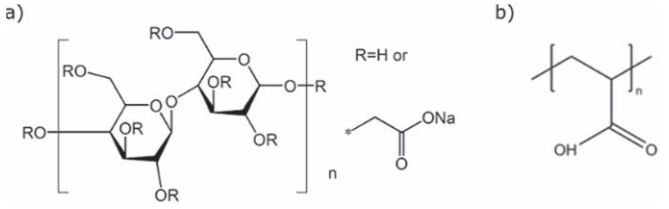

Figure 1. Chemical structures of (a) CMC and (b) PAA polymers.

used limited mass-loadings of the electrode or been limited to investigations in half-cells. Previous research has shown that conclusions made from such experiments cannot automatically be transferred to more realistic LIB cell formats.[28] Moreover, the role of PAA in LNMO positive electrodes is still not well understood during electrode fabrication, cycling and ageing. The objective of this study is therefore to gain a better understanding of the role of PAA as a binder in comparatively thick LNMO electrodes used in full-cells with graphite, thereby approaching industrial standards.

Experimental

Materials.—LNMO powder (TBM-129, average diameter 5–-20 μm, Haldor Topsoe A/S), polyacrylic acid (PAA, 35 wt% solution in water, average M_w = 250,000, Sigma Aldrich), sodium carboxymethyl cellulose (CMC, Leclanché), super P C65 (Imerys), and carbon-coated aluminium foil (20 μm thick, SDX, Showa Denko) were used as received. Microporous monolayer Celgard 2500 separators were cut into 4 × 4 cm dimensions and were dried at 70 °C for 5 h under vacuum. Li-metal foil (125 μm, Cyprus Foote Mineral) was used as received and was stored in an argon environment. Graphite electrodes (Haldor Topsoe, 1.8–2 mAh cm^{-2}) were cut into 22 mm diameter discs and dried for 12 h under vacuum in a Büchi oven at 120 °C. 1 M lithium hexafluorophosphate ($LiPF_6$) in 1:1 ethylene carbonate:diethyl carbonate (EC:DEC, (w/w), LP40, Gotion) was used as the electrolyte as received, stored under argon.

Electrode preparation and cell assembly.—The ratio used to prepare the electrodes were 90 wt% LNMO, 5 wt% carbon black, and 5 wt% binder (i.e., either CMC or PAA). Distilled water was used as the solvent for electrode preparations. The slurry was thoroughly mixed using a shaker ball mill for 30 min at 25 Hz, followed by casting onto a carbon-coated aluminium foil using a doctor blade with a wet thickness of 500 μm. The LNMO electrodes were dried at 70 °C for 12 h. The active mass loading of the electrodes was roughly 10 mg cm^{-2} (~1.5 mAh cm^{-2}) unless otherwise specified. The electrodes were cut into 20 mm discs, followed by calendaring at 5 tons for 3 min using a hydraulic press. These electrodes were then dried under vacuum at 120 °C in a Büchi oven for 12 h.

The cells were assembled in a pouch cell format, unless stated otherwise, in an argon-filled glove box that was kept at an O_2 and H_2O level of less than 1 ppm. For full-cell tests, the LNMO electrodes were tested against graphite electrodes, while they were tested against lithium for half-cells. 120 μl of LP40 electrolyte was used in full-cells, with two Celgard separators placed between the working and counter electrodes.

Galvanostatic cycling with intermittent current interruption technique.—The full-cells were galvanostatically cycled on an Arbin BT-2043 cycling equipment. The cells were kept at open circuit conditions for 10 h before the cycling was performed. The cycling voltage range was from 3.5 V to 4.8 V and was performed at room temperature, with the first three cycles at a C/10 rate and a C/3 rate for the remainder of the cycles. All stated voltage values refer to the Li/Li$^+$ redox couple and the charge-discharge rate of 1 C is equivalent to a specific current of 147 mA g^{-1}. For the intermittent current interruption (ICI) measurements, a pause of 1 s was made every 5 min, and voltage responses were recorded at 0.1 s. The analysis was carried out using a protocol established by M.J. Lacey.[29]

Surface characterization.—The surface morphology of the electrodes was examined using a Zeiss 1550 field emission secondary electron microscope (FE-SEM). To minimize the impacts of charging and binder breakdown on the electrode surfaces, secondary electron microscopy (SEM) images were taken at an accelerating voltage of 5 kV. All measurements were conducted at a 5 mm working distance.

Ion milling.—The cross-sectioning of the LNMO electrodes was performed through argon ion milling technique, using a Gatan Ilion II ion polisher. The electrode was attached to a carbon substrate that was fixed to the holder of the ion polisher. The acceleration voltage was set to 6 keV and the milling duration was 5 h. After the milling process, the electrode was examined using SEM.

Rheological measurements.—The rheological analysis was performed with a Discovery Hybrid Rheometer 2 from TA Instruments with a 40 mm and 2.0125° aluminum cone plate geometry. Oscillation frequency sweep measurements were performed with 1% strain in the frequency range 0.01–10 Hz at 25 °C in air.

In-situ impedance.—A VMP3 potentiostat/galvanostat (BioLogic) was used to carry out electrochemical impedance spectroscopy measurements in LNMO half-cells that contained either PAA or CMC binders. The cells were rested for a period of 10 h prior to the experiment. The impedance spectra were recorded during the cycling procedure, which was as follows: the cells were cycled at a C/10 rate for three formation cycles in the voltage range of 3.5 to 5.0 V. After the third discharge step, the potential was held for one hour at 2.5 V, after which an impedance spectrum was obtained. The impedance spectra were obtained in the potential controlled mode with a peak-to-peak amplitude of 15 mV in the 100 kHz to 100 mHz frequency range. The cells were then further cycled at a C/3 rate for 10 cycles before obtaining an impedance spectrum again. This step was repeated five times. The capacitance values from the EIS spectra were calculated according to the procedure developed and validated by Oswald et al.[30]

Pressure evolution studies.—Pressure monitoring was performed in a helium-leak tested pressure cell (PAT-Cell-Press, El-Cell® GmbH, Germany) and guaranteed a maximum leakage rate of 0.3 mbar/hour. The PAT-Cell-Press consists of a lower plunger, upper plunger and insulation sleeve which were all used as delivered by El-Cell. The plungers are respectively made of aluminum and copper, acting as current collectors. The insulation sleeve contained a pre-dried 260 μm borosilicate-glass fiber separator with a diameter of 18 mm (GF/A of Whatman®, United Kingdom). All electrodes were punched to a diameter of 18 mm and dried under vacuum at 120 °C. The cells were assembled with 100 μl LP40 electrolyte in an argon-filled glovebox (MBraun) with O_2 and H_2O levels less than 1.0 ppm. After assembly, the cells were placed in a climate chamber (KB53, Binder® GmbH) and cycled at 30 °C using a Biologic potentiostat. These cells were cycled for 3 formation cycles only, between 3.5 V and 4.8 V.

Results

Cycling performance using ICI.—ICI measurements were performed on LNMO electrodes that contained either CMC or PAA binder, allowing for simultaneous monitoring of internal resistance changes during the galvanostatic cycling measurements by a repeated brief interruption of the current load. The ICI tests were carried out at room temperature for the LNMO-graphite full-cells. The LNMO electrodes had ~10 mg cm^{-2} of active mass loading. The first column in Fig. 2 displays, in a top-down order, the

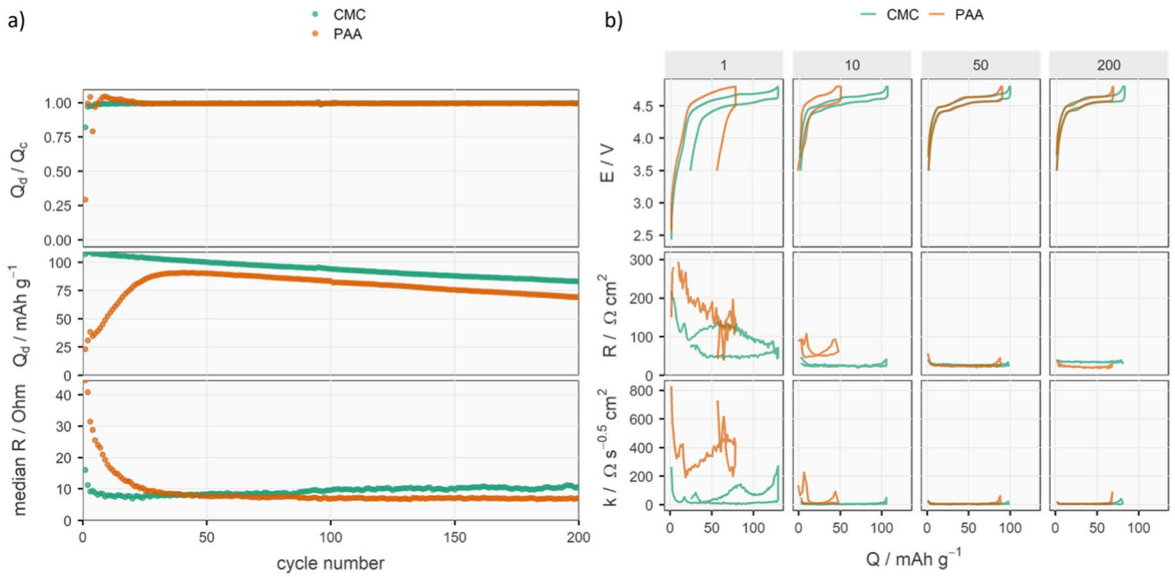

Figure 2. ICI data for LNMO-graphite full cells using either CMC or PAA as binder. From top to down: figure (a) shows CE, discharge capacity and median resistance. From top to down: figure (b) displays the voltage profile, resistance curves and the diffusion coefficients of cycle 1, 10, 50 and 200. See Fig. S1 for a zoomed-in version of R and k values of cycles 10, 50, and 200.

coulombic efficiency (CE), discharge capacity, and median resistance with respect to the cycle number. The second column depicts the potential profile, internal resistance (R), and lithium diffusion resistance coefficient (k) at cycles 1, 10, 50, and 200. Cells utilizing PAA as the binder exhibit poor initial CE and discharge capacity, only ∼29%, and ∼23 mAh g^{-1} respectively in the first cycle. These results align with a high internal resistance in the first cycle, as indicated by the resistance results. The limited capacity of the PAA cells, shown by the voltage profiles for cycles 1 and 10, indicates that the high resistance is a significant factor contributing to the low capacity. The sloping voltage profile and the absence of a well-defined endpoint at the end of the 1st and 10th charge cycle indicate that there is a substantial iR drop within the electrode which is restricting the charging process.[2] The high internal resistance results in a drop in the cell voltage, leading to an early shutdown of the cell before the full capacity is achieved. The high R and k values in both the 1st and 10th cycles of the PAA cell, compared to the CMC cell, indicate higher internal resistance and reduced mobility of the Li ions. This supports the low discharge capacity obtained in the PAA cell. The cell with CMC binder on the other hand shows an initial CE of ∼83% and an initial discharge capacity of 116 mAh g^{-1}, which is within the range of what is typically observed in LNMO full-cells and retains about 73% of its initial capacity after 200 cycles. The CMC based cell also shows a relatively lower initial internal resistance, which is then more or less constant with increasing number of cycles compared to the PAA based cell.

A comparison of the electrochemical performance was carried out on LNMO electrodes with both low (4.9 mg cm^{-2}) and high (11.7 mg cm^{-2}) active mass loadings to examine any variations in their performance. The results are presented in Fig. 3. During the first 25 cycles (see Fig. S2 for data up to 200 cycles), a substantial difference in electrochemical performance was noted. The cell with a high mass loading, referred to as "PAA-high," has a lower initial CE of ∼29% and a first cycle discharge capacity of 23.1 mA h g^{-1}, compared to the cell with a low mass loading, referred to as "PAA-low," which has a CE of ∼68% and a discharge capacity of 86.1 mA h g^{-1}. The extremely low CE and discharge capacity for the higher loading is likely due to the high internal resistance in the cell, as stated in the previous section, and is also demonstrated by a significant iR drop in the voltage profile shown in Fig. 3a. A gradual increase in discharge capacity for PAA-high is clearly visible during the first 25 cycles and is accompanied by a corresponding decrease

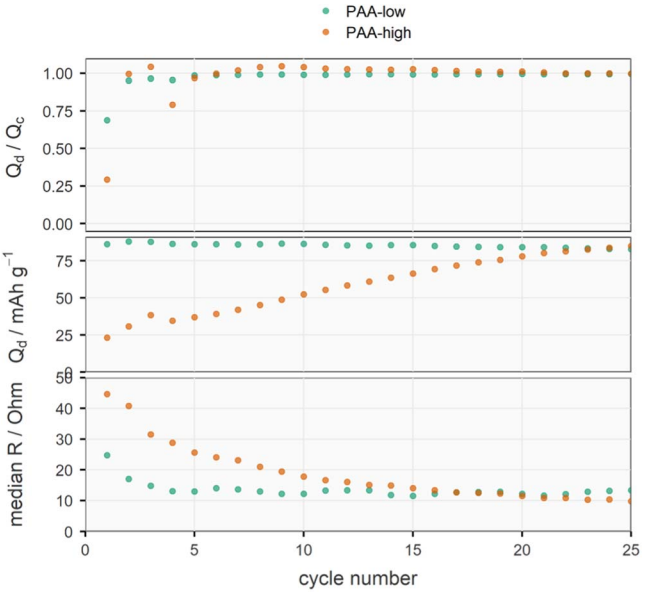

Figure 3. From top-to-bottom CE, discharge capacity and median resistance up to 25 cycles for cells with PAA binder in low and high electrode loading.

in the median resistance. In combination with an inadequate wetting of the electrode and low electrolyte permeability, these negative effects become apparent at a higher mass loading of the electrode. This would explain the increasing capacity during longer cycling time.

Morphology analysis.—The SEM micrographs of the pristine thick LNMO electrodes after drying at 70 °C in vacuum and before calendaring are shown in Fig. 4. LNMO active particles with an average diameter of 5–20 μm are clearly observed in these images. Figure 4a reveals the homogeneity of the electrode components in the electrode that uses CMC binder, while cracks are noticeably present in the electrode using PAA binder, as seen in Fig. 4b. The presence of cracks in the electrode reduces the electronic transfer ability between active particles and overall electrode conductivity, causing a decrease in the electrochemically active area due to the

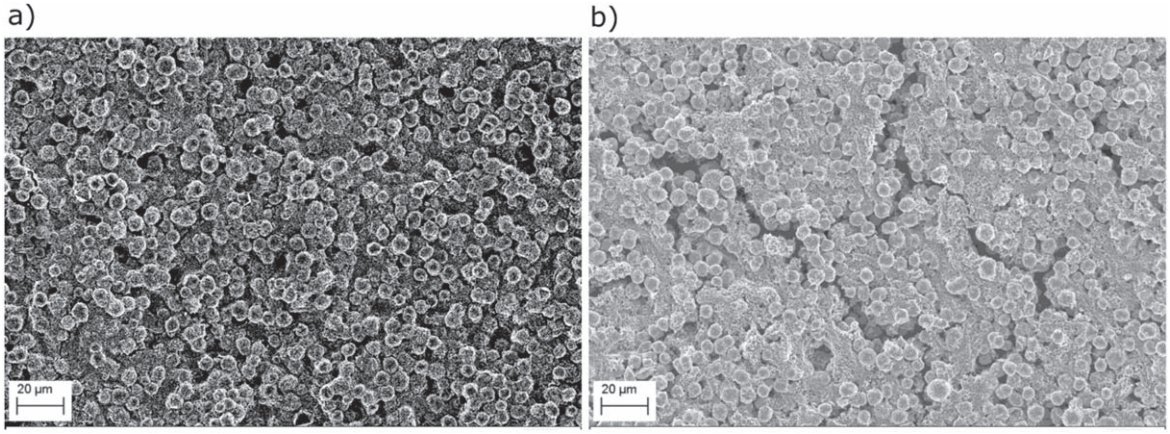

Figure 4. SEM images of LNMO electrodes using (a) CMC and (b) PAA binder.

lower supply of electrons, ultimately resulting in a decreased electrochemical performance.[31] It is important to note that the electrodes utilized in the galvanostatic cycling tests were processed through calendaring prior to the assembly of the cell, which could potentially decrease the size of the cracks.[31]

An explanation for the cracks in the electrode material might be due to the capillary pressures at the interface between the particles and the solvent in the slurry. The capillary pressures are formed during the drying process and increase the more the solvent evaporates, until a critical point when it is released and cracks are formed.[32] The capillary pressure at the interface of the particles and water is affected by the surface tension of the water in the slurry and is less pronounced and alleviated when the surface tension is low. Another reason can be evolution of hydrogen gas during the drying process of water-based slurries due to oxidation of the aluminium current collector because of increased pH.[33,34] However, since aluminium current collectors were used for all LNMO electrodes, the different appearance (in terms of cracks) between for the CMC and PAA samples most probably arise from different capillary pressures during the drying process. Although rheological measurements rather determine the bulk properties of compounds, they can help to explain the different appearances of the LNMO slurries. In Fig. 5, the rheological response for the storage (G') and loss (G'') moduli are presented for LNMO slurries with PAA and CMC binders respectively. The drying process, when the capillary pressures are formed, is a relatively slow process and can be translated to the low-frequency response in an oscillation frequency sweep measurement, where the deformations are slow. As seen in Fig. 5, the PAA-based slurries have a dominant G' response at low frequencies, implying that a more solid-like and elastic behaviour is pronounced, suggesting that more interactions are present which keeps the particles together during slow deformations. For CMC on the other hand, the G'' response is dominant independent of the frequency, indicating the material flows during deformation. The dominant G' response for PAA stems from the higher concentration of functional groups which cross-links the system to a higher degree. These interactions support the generation of cracks since the particles are less accessible for deformation and relaxation during drying and therefore promote the build-up of capillary pressures. Interestingly, these results contradict the behaviour observed for PAA and CMC in simple water solutions,[35] indicating that electrode slurries are complex, and more interactions are present that affects their overall behaviour.

The cross-section SEM images shown in Fig. 6 were obtained by performing ion milling on the pristine LNMO electrodes. Figure 6b demonstrates a strikingly uneven distribution of LNMO particles, carbon black, and the PAA binder. In some areas, there is an agglomeration of carbon black and/or PAA binder, suggesting poor electronic wiring and that the electrode slurry was not mixed as well

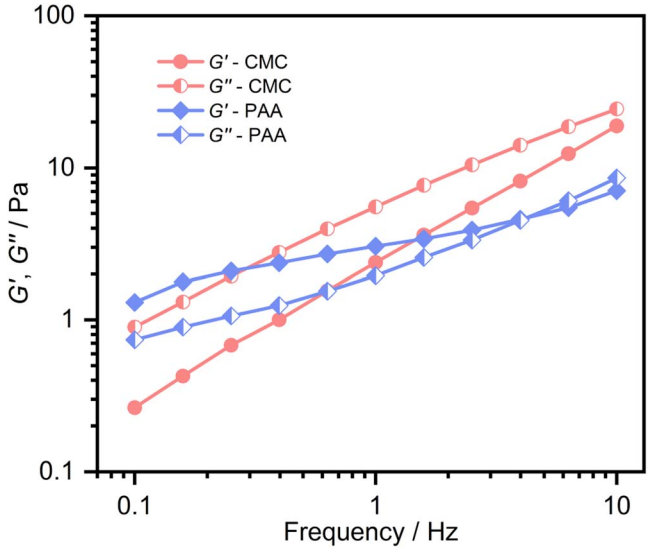

Figure 5. Oscillation frequency sweep of LNMO electrode slurries with CMC and PAA as binder.

during processing as the CMC electrodes displayed in Fig. 6a. This could be due to a non-uniform distribution of the binder resulting from intermolecular and intramolecular interactions between the carboxyl units in PAA,[36] which can cause the formation of coiled and compact structures that may lead to clogging in certain areas of the electrode. Since ion milling is a destructive method, it is not possible to rule out the chance of directly removing hard or soft materials from the electrode during the milling process, restricting direct observation of the electrode, but there are nevertheless obvious differences between the two binder types. Another significant distinction between the two electrodes is that the LNMO particles near the current collector or situated deeper into the bulk of the electrode in the PAA-based electrode have limited contact with the conductive carbon and/or binder in comparison to those in the CMC-based electrodes.

In-situ impedance studies.—The in situ impedance studies were performed in LNMO half-cells in blocking conditions to monitor the change in the electrochemically active surface area of the LNMO electrode upon cycling according to the procedure developed and validated by Oswald et al.[30] They used their analysis of the low-frequency domain of the EIS spectra to establish the capacitance values at both 180 mHz and a phase angle above 0.85, and also performed a Brunauer–Emmett–Teller (BET) surface area analysis for confirmation of their results.

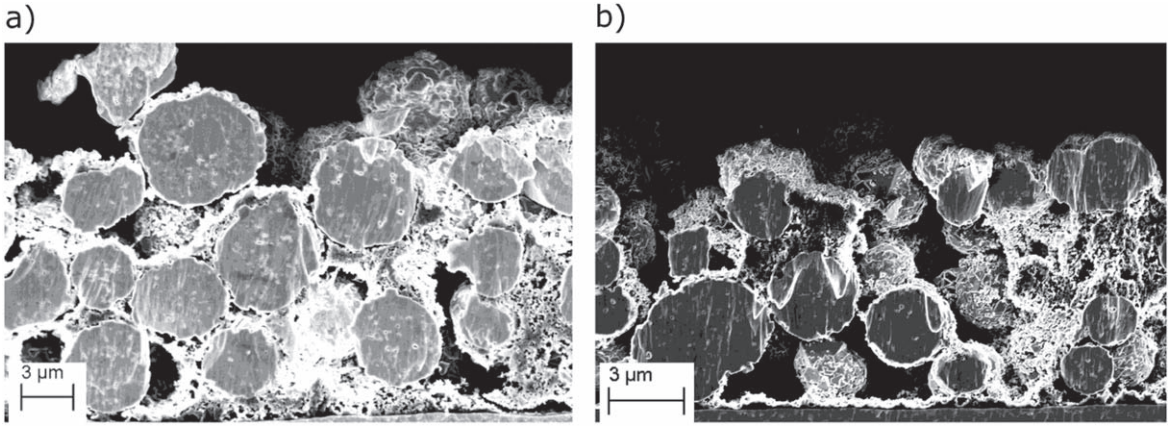

Figure 6. Cross-section SEM images of LNMO electrodes after ion milling: (a) electrode with CMC binder, (b) electrode with PAA binder.

In the experiments carried out within the present study, the electrochemical double layer capacitance was estimated and is correlated to the active surface area of the LNMO electrode. The equivalent circuit model presented in Fig. S4 was used to fit the EIS spectra, and the estimated capacitance values calculated using a single measurement from ~180 mHz using the equation below are shown in Table I:

$$Q \approx \frac{1}{\omega_o.(-\mathrm{Im}(Z\omega_o))}$$

In this study, the phase angle in the CMC cell ranges from 0.42 to 0.54, whereas in the case of the PAA cell, it ranges from 0.58 to 0.64. This indicates a higher error rate when estimating capacitance than at a phase angle of 0.85, as mentioned in the referred article.

The capacities of the electrodes are directly related to their electrochemically active surface area. When analysing Table I, the estimated capacitance is generally higher for the LNMO cell that uses CMC as binder compared to the one that uses PAA. This suggests that the electrode with CMC binder has a larger electrochemically active surface area, indicating that the CMC binder does not block the surface of the LNMO electrode. For the PAA-based cell, the capacitance values are approximately less than half of those in the CMC-based cell. This suggests that a relatively smaller electrochemically active surface area is exposed, likely due to higher coverage of the PAA binder which blocks the active surface. The estimated capacitance values for the CMC-based cell show no obvious trend when observed during multiple cycles but remains fairly stable. For the PAA-based cell, however, a noticeable increase in capacitance can be seen from the 11th to the 22nd cycle, which then remains relatively constant for subsequent cycles. The findings from the PAA-based cells suggest that the electrochemically active surface area increases up to around the 22nd cycle. This implies that the coverage of the PAA binder on the LNMO active surface is decreasing up to this number of cycles, and thereafter remains during further cycling. These findings are consistent with the results from the ICI measurements, which show that the initial capacity of the PAA cell is lower, but gradually increasing during cycling. This may be because of the uneven distribution of PAA in LNMO, leading to more binder at the surface, and thereby poor Li-ion conduction.

Moreover, after examining the high-frequency region of the EIS spectra, a semi-circle was identified that is typically associated with charge-transfer resistance and resistances originating from interphase or contact. However, since the EIS measurements were conducted under blocking conditions, the chance of charge transfer resistance can be eliminated, and the results can instead be attributed to interphase resistance, contact resistance, or both. Figure 7 shows the EIS spectra of both CMC- and PAA-based cells. A significant difference that can be observed when examining the high-frequency parts of the EIS spectra of these two cells is that the diameter of the semi-circle in the CMC based cell progressively grows as the cell cycles, increasing from 83.6 $\Omega\ cm^2$ in the 11th cycle to 94.1 $\Omega\ cm^2$ in the 55th cycle, thus indicating a growing resistance. In the 11th cycle, the PAA cell displays a value of 93.4 $\Omega\ cm^2$ which decreases as cycling progresses and eventually stabilizes. This indicates that the resistance of the PAA cell decreases over time and stabilizes after 25 cycles. These findings are also consistent with the ICI results, which indicate that the resistance values decrease and stabilize after a certain number of cycles.

Pressure evolution studies.—During the formation cycles, the electrolyte is being reduced at the anode and oxidized at the cathode sides, respectively. This electrolyte decomposition results in the formation of a passivating, ionically conducting and electronically insulating layers (commonly named solid electrolyte interphase (SEI) on the anode and cathodic electrolyte interphase (CEI) on the cathode). Although these electrolyte/electrode reactions are to some extent beneficial, they can also lead to the formation of undesired gaseous, solid, and liquid products, which can contribute to cell failure. Recent *operando* studies have shown the evolution of gaseous decomposition products in LNMO-graphite cells, using both online and differential electrochemical mass spectrometry.[37–39] However, these setups remove the gas products that are formed during cycling. In the alternative setup used here, the gases remain within the battery cell and can therefore mimic realistically operating batteries. It should be noted, however, that with this setup it is not possible to qualitatively analyse the gases *operando*.

Table I. Changes in the estimated capacitance over cycling for LNMO half-cells using either CMC or PAA binders.

Cycle number	CMC—Estimated capacitance (F)	PAA—Estimated capacitance (F)
11	0.0051	0.0021
22	0.0060	0.0026
33	0.0056	0.0027
44	0.0059	0.0028
55	0.0060	0.0028

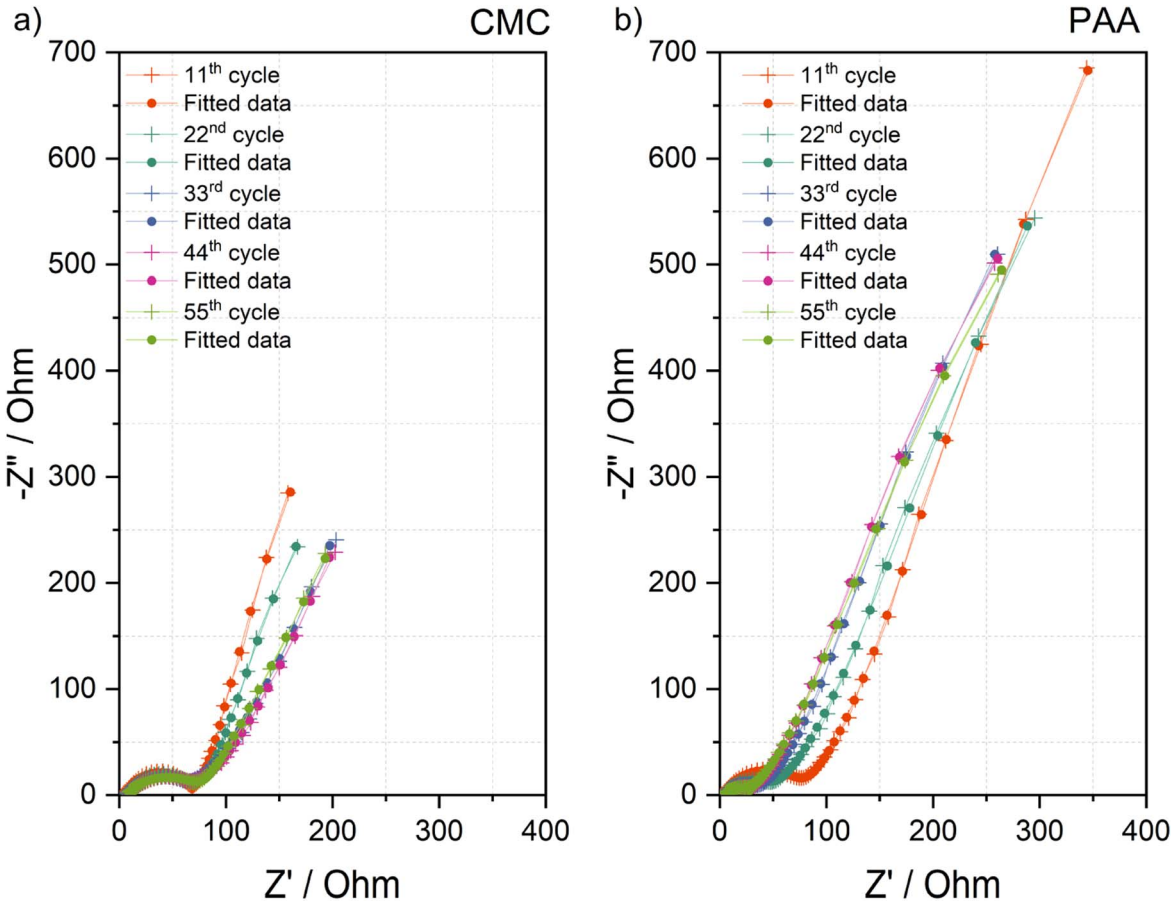

Figure 7. EIS spectra during cycling for LNMO half-cell using (a) CMC and (b) PAA binders.

In Fig. 8 the time-dependent full-cell potential and corresponding pressure curve are shown for the formation cycles in a LNMO-graphite cell with different binders for the LNMO electrode. The pressure increase in LNMO with the CMC binder is approximately 6

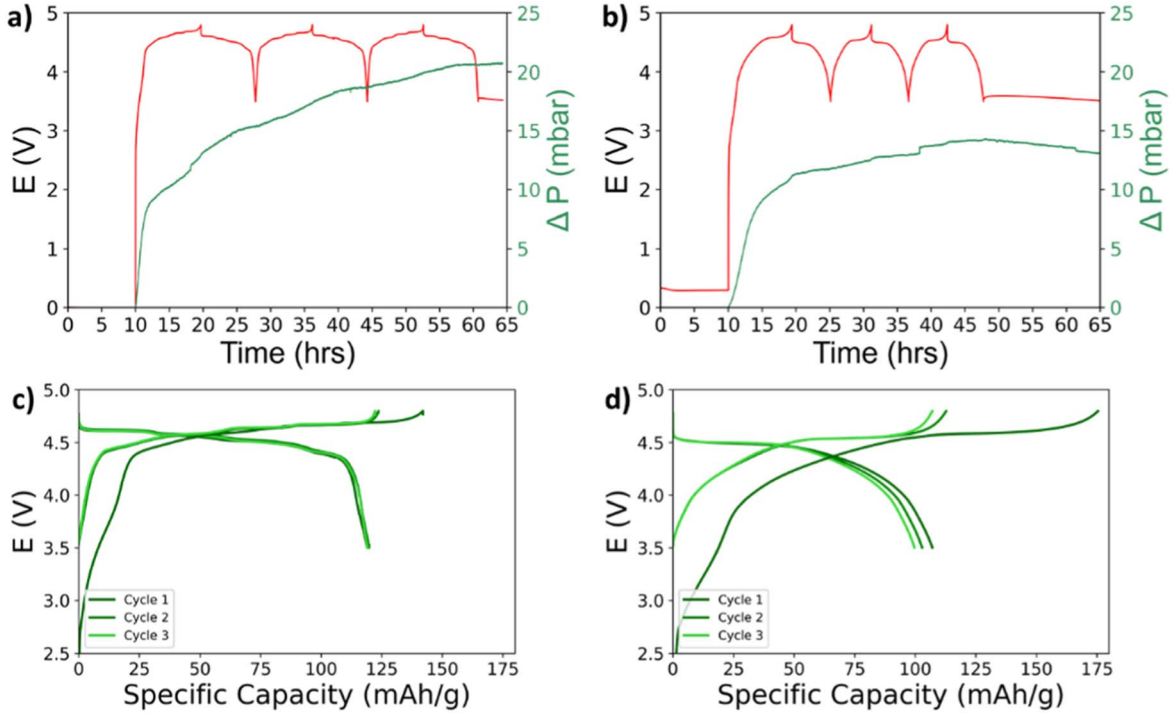

Figure 8. Pressure evolution curves during formation cycling of cells using LNMO electrodes with (a) CMC binder and (b) PAA binder. Capacity curves of the same cells using (c) CMC binder and (d) PAA binder.

mbar higher than for LNMO with the PAA binder. It can thus be deduced that the reactions during the formation cycles with the PAA binder cause a lower volume of gases. Nevertheless, it should also be mentioned that the pressure evolution in the first charge cycle is rather similar for both CMC and PAA binders. An increase of about 12 mbar is observed during the first charge, indicating a similar initial formation of CEI and SEI, as observed in an earlier work by our group.[40] However, in the subsequent cycles, the pressure evolution seems to stabilize for PAA, whereas it continues to increase for the CMC binder. From the capacity curves, in Figs. 8c and 8d, it can be observed that LNMO with CMC binder has more stable cycling than LNMO with PAA binder. This suggests that the degradation reactions in the formation cycles not only result in the formation of favourable SEI and CEI components but are also accompanied with the formation of gaseous species. The chemical reactivity of the CMC binder is also in agreement with earlier studies, where its reactivity toward the electrolyte has been attributed to the reactive hydroxyl groups at the surface, contributing to the formation of a stable passivation layer.[41] This may explain the increased pressure evolution of CMC binder and better irreversible capacity of CMC, compared to PAA.

Discussion

The use of PAA and/or its Li- or Na-salts as a binder for lithium-ion battery electrodes has been investigated across various battery chemistries including silicon nanoparticle-based electrodes,[9] graphite,[42,43] $LiFePO_4$,[44] LNMO,[45] Ni-rich layered oxide cathodes,[11] among others, highlighting the applicability of these materials as binders. It has an ability to create hydrogen bonds with the active material, and thereby limit the contact with the electrolyte. PAA has therefore been used also in this study, but with LNMO electrodes that have a higher mass loading than those in other studies. The findings presented here, however, indicate that PAA is not an effective binder in LNMO electrodes with high mass loading, making it largely unsuitable for use in LNMO cathodes. A higher internal resistance in the cells, particularly during the initial cycles was observed for PAA-based cells compared to CMC-based cells.

PAA has carboxylic acid functional groups, while CMC has carboxymethyl groups. Differences in the concentration of functional groups and interactions—both intermolecular and intramolecular—among the carboxyl units in PAA, which can result in coiled and compact structures, could lead to performance variations when compared to the CMC binder. From the literature, it is claimed that the PAA polymer undergoes agglomeration in water due to hydrogen bonds between its carboxylic groups, whereas the Li salts of PAA have more extended polymer chains due to the electrostatic repulsion between their carboxylate groups.[22] In contrast, our findings when using Na-PAA as a binder for thick LNMO slurry coatings (see Fig. S5) showed that the electrodes have numerous cracks after vacuum drying, rendering further analysis inadequate. Chong et al. reported that the use of neutralized Li-PAA and Na-PAA resulted in improved performance, in both graphite and $LiFePO_4$ electrodes, including better CE during the first cycle, a smoother electrode surface after cycling, and a longer cycle life.[46] They emphasized the significance of adding an adequate amount of styrene-butadiene rubber (SBR) to compensate for the brittleness of polyacrylates—another distinct chemical property resulting from differences in molecular structure compared to CMC. This is similar to the commonly used practice with Na-CMC. They also pointed out that increasing the amount of elastomer led to a gradual decrease in electronic conductivity.[10,46] The literature also suggests that PAA differs from the commonly used binder, PVdF, in that it does not undergo significant swelling in the electrolyte. As a result, it maintains better adhesion and protects the surface of the active particle by acting as an artificial SEI/CEI,[10] but could also be a reason for crack formation.

Our results indicate that PAA and its Na- or Li-derivates may not be the best choice for all the crucial binder properties in an LNMO electrode. Nonetheless, it cannot be ruled out that these materials have the potential to be optimized for use in advanced batteries, leading to improved performance. Since PAA has a high concentration of carboxyl groups, some polymer properties such as adhesion strength, surface chemistry, and swelling in the electrolyte, can in principle be controlled by copolymerization with suitable functionalities. Through further tailoring of the polymer chemistry, the intermolecular and intramolecular interactions in the polymer which cause agglomerations and eventual clogging of the electrode pores could be avoided. Additionally, the inclusion of other binders such as SBR can help compensate for the brittleness of polyacrylates and improve the overall properties of the binder.[47] In the future, extended efforts will be required to gain a more complete understanding, together with post-cycling characterizations, to further comprehend its microstructural and mechanical property changes with cycling and how they affect the electrochemical performance, providing effective guidance for practical applications. These should preferably incorporate tests also at higher mass loadings.

Conclusions

The electrochemical performance of high mass loading LNMO electrodes using PAA as binder was investigated and compared to CMC binder in full-cells with graphite electrodes. Despite promising results in the literature for PAA with many battery electrodes, including LNMO, the cells using PAA as a binder have here exhibited subpar electrochemical performance in terms of discharge capacity, mainly because of the high internal resistance within the cell. Additionally, surface analysis of the electrode using PAA binder showed substandard electrode properties such as poor binder distribution. These findings highlight the need for further research into the factors that govern material compatibility in LNMO electrodes, particularly at high mass loadings.

Acknowledgments

We thank Haldor Topsoe for providing the LNMO powder and graphite electrodes. The impartial financial support provided by Volkswagen AG and Scania CV AB is gratefully acknowledged. The support provided by the STandUP for Energy consortium, from Batteries Sweden through Vinnova, and from CoFBAT, which is an EU-funded project that has received funding from the European Union's Horizon 2020 Research and Innovation Programme under Grant Agreement n. 875126 are acknowledged. We acknowledge Myfab Uppsala for providing facilities and experimental support. Myfab is funded by the Swedish Research Council as a national research infrastructure. Dr. Saravanan Karuppiah is acknowledged for helpful discussions.

ORCID

Rassmus Andersson https://orcid.org/0000-0002-0879-7603
Reza Younesi https://orcid.org/0000-0003-2538-8104
Daniel Brandell https://orcid.org/0000-0002-8019-2801

References

1. G. Liang, V. K. Peterson, K. W. See, Z. Guo, and W. K. Pang, *J Mater Chem A Mater*, **8**, 15373 (2020).
2. A. Mathew et al., *Batter Supercaps*, **5**, e202200279 (2022).
3. F. Ulu Okudur et al., *J. Alloys Compd.*, **892**, 162175 (2022).
4. S. Lee and A. Manthiram, *ACS Energy Lett.*, **7**, 3058 (2022).
5. B. Aktekin et al., *J. Phys. Chem. C*, **122**, 11234 (2018).
6. E. R. Østli et al., *ACS Omega*, **6**, 30644 (2021).
7. J. C. Hestenes, J. T. Sadowski, R. May, and L. E. Marbella, *ACS Mater. Au*, **3**, 88 (2022).
8. B. T. Young et al., *J. Mater. Res.*, **34**, 97 (2019).
9. P. Parikh et al., *Chem. Mater.*, **31**, 2535 (2019).
10. D. Bresser, D. Buchholz, A. Moretti, A. Varzi, and S. Passerini, *Energy Environ. Sci.*, **11**, 3096 (2018).
11. F. Reissig et al., *ChemSusChem*, **15**, e202200401 (2022).
12. P. Mu et al., *J. Am. Chem. Soc.*, **143**, 18041 (2021).
13. F. Jeschull et al., *ACS Appl. Energy Mater.*, **1**, 5176 (2018).
14. F. Jeschull et al., *J. Power Sources*, **325**, 513 (2016).

15. L. Rao et al., *ACS Appl. Mater. Interfaces*, **14**, 861 (2022).
16. A. Mistry et al., *J. Electrochem. Soc.*, **168**, 070536 (2021).
17. M. J. Lacey et al., *ChemSusChem*, **10**, 2758 (2017).
18. X. Zhong et al., *Appl. Surf. Sci.*, **553**, 149564 (2021).
19. V. A. Nguyen and C. Kuss, *J. Electrochem. Soc.*, **167**, 065501 (2020).
20. T. Kocak, X. Qi, and X. Zhang, *Solid State Ion*, **383**, 115989 (2022).
21. G. D. Salian et al., *ChemistryOpen*, **11**, e202200065 (2022).
22. W. Porcher et al., *J. Electrochem. Soc.*, **164**, A3633 (2017).
23. Z. Karkar, D. Guyomard, L. Roué, and B. Lestriez, *Electrochim. Acta*, **258**, 453 (2017).
24. S. J. Choi et al., *ACS Sustain Chem Eng*, **4**, 6362 (2016).
25. J. Sun et al., *J. Alloys Compd.*, **783**, 379 (2019).
26. Z. P. Cai, Y. Liang, W. S. Li, L. D. Xing, and Y. H. Liao, *J. Power Sources*, **189**, 547 (2009).
27. Q. Zhang et al., *Mater Today Energy*, **29**, 101128 (2022).
28. F. Jeschull, D. Brandell, M. Wohlfahrt-Mehrens, and M. Memm, *Energy Technology*, **5**, 2108 (2017).
29. M. J. Lacey, *ChemElectroChem*, **4**, 1997 (2017).
30. S. Oswald, D. Pritzl, M. Wetjen, and H. A. Gasteiger, *J. Electrochem. Soc.*, **167**, 100511 (2020).
31. B.-S. Lee et al., *J. Electrochem. Soc.*, **165**, A525 (2018).
32. Z. Du et al., *J. Power Sources*, **354**, 200 (2017).
33. I. Dienwiebel et al., *Advanced Energy and Sustainability Research*, **2**, 2100075 (2021).
34. R. Sahore et al., *ACS Sustain Chem Eng*, **8**, 3162 (2020).
35. R. Y. Z. Hu, A. T. A. Wang, and J. P. Hartnett, *Exp. Therm Fluid Sci.*, **4**, 723 (1991).
36. A. M. F. Alhalawani, D. J. Curran, D. Boyd, and M. R. Towler, **36**, 221 (2016).
37. B. Michalak et al., *Anal. Chem.*, **88**, 2877 (2016).
38. S. Solchenbach, M. Wetjen, D. Pritzl, K. U. Schwenke, and H. A. Gasteiger, *J. Electrochem. Soc.*, **165**, A512 (2018).
39. Z. Jusys, M. Binder, J. Schnaidt, and R. J. Behm, *Electrochim. Acta*, **314**, 188 (2019).
40. G. D. Salian et al., *Batter Supercaps*, **6**, e202200565 (2023).
41. L. El Ouatani et al., *J. Power Sources*, **189**, 72 (2009).
42. S. Komaba, T. Ozeki, and K. Okushi, *J. Power Sources*, **189**, 197 (2009).
43. S. Komaba et al., *J. Power Sources*, **195**, 6069 (2010).
44. Z. Zhang et al., *Electrochim. Acta*, **80**, 440 (2012).
45. N. P. W. W. Pieczonka et al., *Adv. Energy Mater.*, **5**, 1501008 (2015).
46. J. Chong et al., *J. Power Sources*, **196**, 7707 (2011).
47. M. J. Jolley et al., *ACS Appl. Energy Mater.*, **6**, 496 (2023).